Advanced Mirror Technology Development (AMTD) thermal trade studies

Thomas Brooks, Phil Stahl, Bill Arnold

ABSTRACT

Advanced Mirror Technology Development (AMTD) is being done at Marshall Space Flight Center (MSFC) in preparation for the next Ultraviolet, Optical, Infrared (UVOIR) space observatory. A likely science mission of that observatory is the detection and characterization of 'Earth-like' exoplanets. Direct exoplanet observation requires a telescope to see a planet that is 10^{-10} times dimmer than its host star. To accomplish this using an internal coronagraph requires a telescope with an ultra-stable wavefront. This paper investigates two topics: 1) parametric relationships between a primary mirror's thermal parameters and wavefront stability, and 2) optimal temperature profiles in the telescope's shroud and heater plate that minimize static wavefront error (WFE) in the primary mirror.

1. Introduction

To directly image an extrasolar planet, a space telescope must be able to differentiate the host star's light from the exoplanet's light. This requires 10^{-10} contrasting. A coronagraph and an extremely stable wavefront make the required contrast achievable. The required level of wavefront stability depends upon the coronagraph and the Zernike composition of the wavefront error. This paper includes two investigations.

For the first investigation, a finite element mesh of a candidate mirror is created and thermal analysis is performed to determine the temperature distribution in the mirror when it is placed inside of an actively controlled cylindrical shroud at Lagrange Point 2. Thermal strains resulting from the temperature distribution are used to determine the WFE to characterize the effect that thermal inputs have on the optical quality of the mirror. This process is repeated for several mirror material properties, material types, and mirror designs to determine how to design a mirror for thermal stability and to determine the relationship between requirements placed on the mirror and requirements placed on the active control system (ACS).

For the second investigation, a finite element mesh of a single mirror is placed into a telescope that has an actively controlled shroud and heater plate. The temperature distributions in the shroud and in the heater plate are varied with the guidance of an optimization algorithm to minimize the RMS WFE of the primary mirror.

2. Active Control Analysis
2.1. Model Layout

2.1.1. Shroud and Scarf

The models are limited to a Kepler-like space telescope architecture as shown in Figure 2. In every case, the outward facing surfaces of the shroud and scarf are covered in MLI (effective emissivity of 0.002; emissivity 0.82) and the inward facing surfaces are covered with black paint (emissivity of 0.91) to prevent stray light from affecting the telescope's optical performance. The shroud and scarf are constrained to a boundary temperature that varies with time to simulate an ACS.

2.1.2. Heated Plate

A heated plate is behind the primary mirror as shown in Figure 2. The plate is made out of Aluminum 6061-T6. The surface of the plate that faces the telescope's shroud is covered in MLI and the mirror facing surface is covered in an optical coating that has an emissivity of 0.9.

2.1.3. Mirror

The mirror's material, conductivity, emissivity, density, and geometry are varied throughout the analyses to determine how those characteristics affect thermally induced WFE stability. The mirror remains 4 meters in aperture, circular, closed back, and with the same light-weighting pattern throughout the analysis as shown in Figure 1. The mirror is made of ULE unless an analysis says that it is made from something else. When material properties are varied, they're varied from the nominal properties shown in Table 1. The properties are static and do not very with temperature, and the mirror's temperature did not vary greatly.
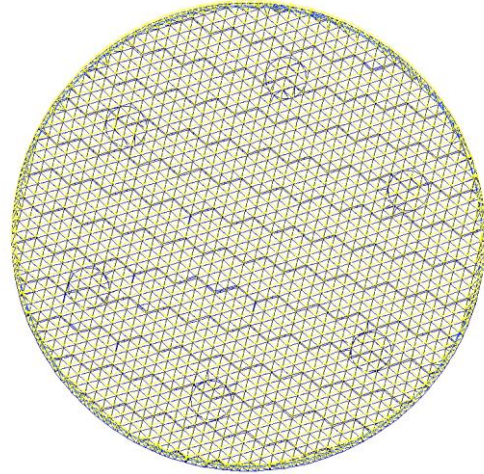

Figure 1: Mirror in Wireframe View

Table 1: Nominal Mirror Properties (ULE)

Conductivity (W/m/K)	Specific Heat (J/kg/K)	Density (kg/m^3)	Emissivity	Rib Thickness (m)	CTE (1/K)
1.31	766	2210	0.82	0.015	30x10^{-9}

2.1.4. Environment

The telescope is placed at Lagrange Point 2 and space's boundary temperature is set to the cosmic microwave background temperature of 2.7K.

2.1.5. Active Control System (ACS)

The ACS in this analysis attempts to maintain the scarf and shroud's temperature at 280K. The scarf and shroud's temperatures are constrained, and modelled as the simple sine wave function shown below and plotted in Figure 3.

$$T(t) = 280 + C \sin\left(\frac{2\pi t}{P}\right)$$

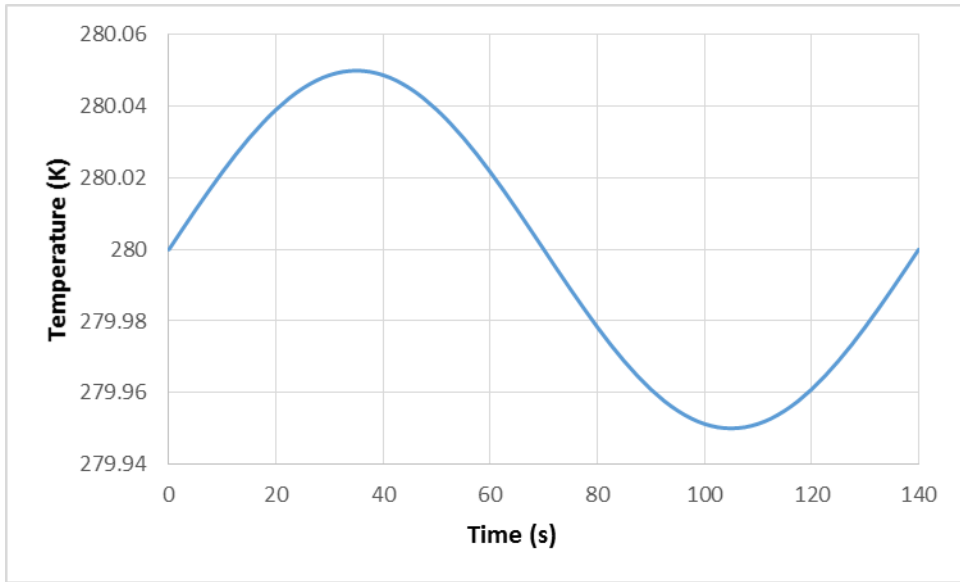Where C is the controllability and P is the period of the ACS.

Figure 3: Temperature of the Shroud and Scarf; 50mK, 140s ACS
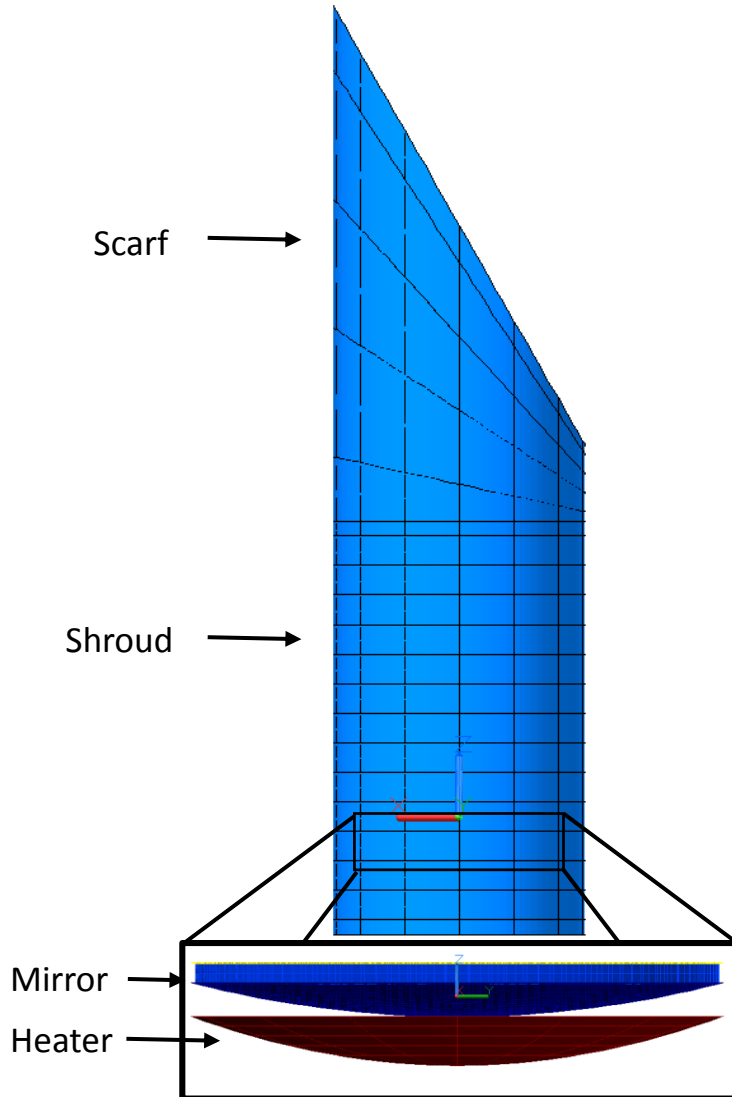

Scarf

Shroud

Mirror

Heater

Figure 2: Space Telescope Architecture

2.2.   Effect of ACS Controllability
2.2.1.Model Setup

The table below contains the values of key quantities in this analysis. This analysis varies the active control system's Controllability, which is the coefficient in front of the sine curve that defines the shroud and scarf's temperature and represents how well the active control system maintains the shroud's temperature at 280K.

Table 2: Effect of ACS Controllability Analysis Settings

Material	ULE
Period of ACS	5000s
Controllability of ACS	Varied
Density of Mirror Material	ULE Density
Emissivity	0.82
Thickness	Nominal
Conductivity	Nominal

A transient analysis is set to run for 50,000s (10 periods) after being initialized in a state that is close to the cyclic steady state of the mirror. The thermal results are post processed and inserted into a NASTRAN thermal expansion analysis using a Python script, and the results of the thermal expansion analysis are processed further to turn deformations into WFE. The initial temperature of the mirror is set to 280K which is the temperature at which the mirror has been polished to be smooth. The controllability of the ACS is varied and set to values of 1mK, 5mK, 10mK, and 50mK to observe trends between the ACS controllability and the range of the RMS WFE.

2.2.2.Model Results

The optical performance of the primary mirror is described with RMS WFE as shown in Figure 4. The stability requirement makes the RMS WFE Range of particular interest, so the range for each controllability is plotted in Figure 5. The ranges in this plot are determined by taking the difference between the maximum WFE and the minimum WFE over one period after the run has reached steady cyclic oscillations.
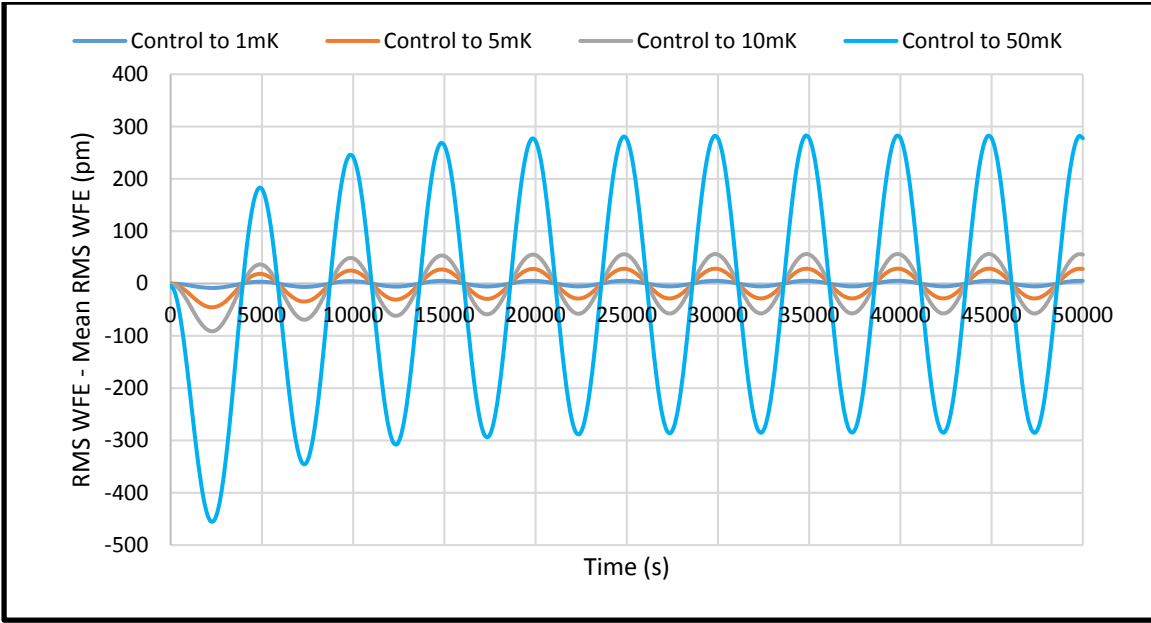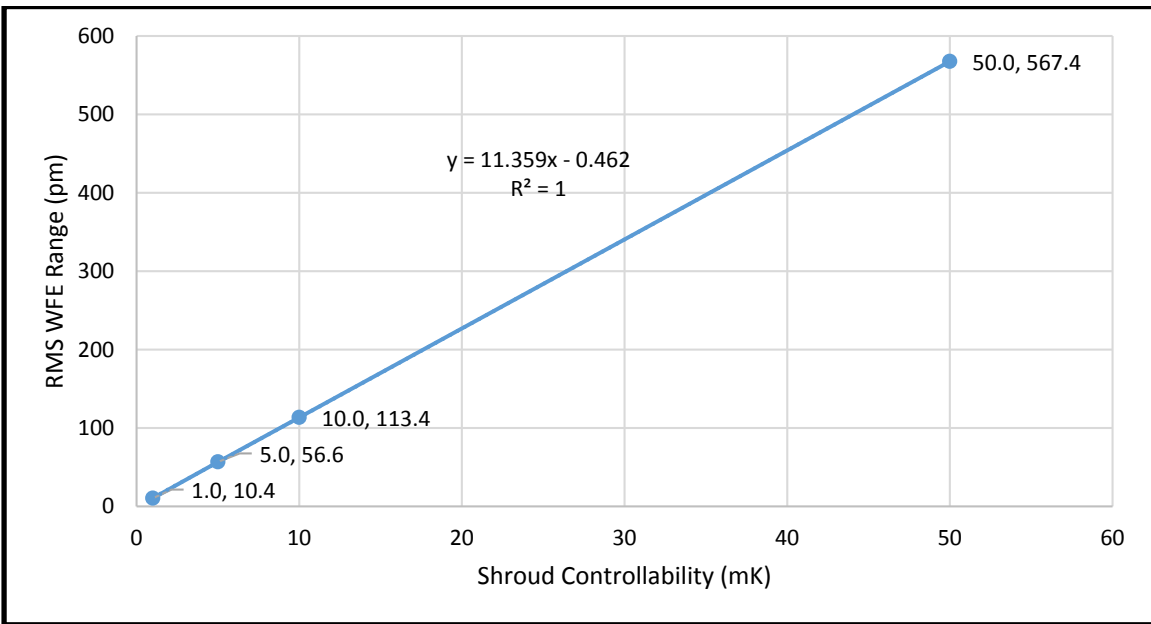
Figure 4: Time versus RMS WFE

Figure 5: Shroud Controllability versus RMS Range

2.2.3. Model Conclusions

There is a linear relationship between Shroud Controllability and the RMS WFE Range. The greater the accuracy of shroud control, the lower the fluctuations in RMS WFE. This general relationship is expected, but the data in this plot (or one like it based on a different configuration) can be used to quantify trade-offs between advanced thermal control and other design solutions.

2.3. Effect of ACS Period
2.3.1. Model Setup

The table below contains the values of key quantities in this analysis. This analysis varies the ACS period of oscillation, which is a number that is affected by the heat capacity of the shroud, the responsiveness of the sensors on the shroud, the sampling rate of those sensors, and the duration of heater cycles.

Table 3: Effect of ACS Period Analysis Settings

Material	ULE
Period of ACS	Varied
Controllability of ACS	50mK
Density of Mirror Material	ULE Density
Emissivity	0.82
Thickness	Nominal
Conductivity	Nominal

Transient cases are run for ACS periods of 3600s, 1800s, 600s, 200s, 140s, 5s, 1s, 0.1s and 0.01s. The duration of the transient runs is 15 times the period of the ACS so that 15 shroud temperature cycles are observed. Only the last 5 cycles are used to avoid using data whose cyclic oscillations have not yet steadied out.

2.3.2. Model Results

The results are summed in a graph that shows the relationship between ACS period and the RMS WFE Range shown in Figure 6. WFE contour plots are presented in Figure 7 and Figure 8 to show which WFE shapes are present.
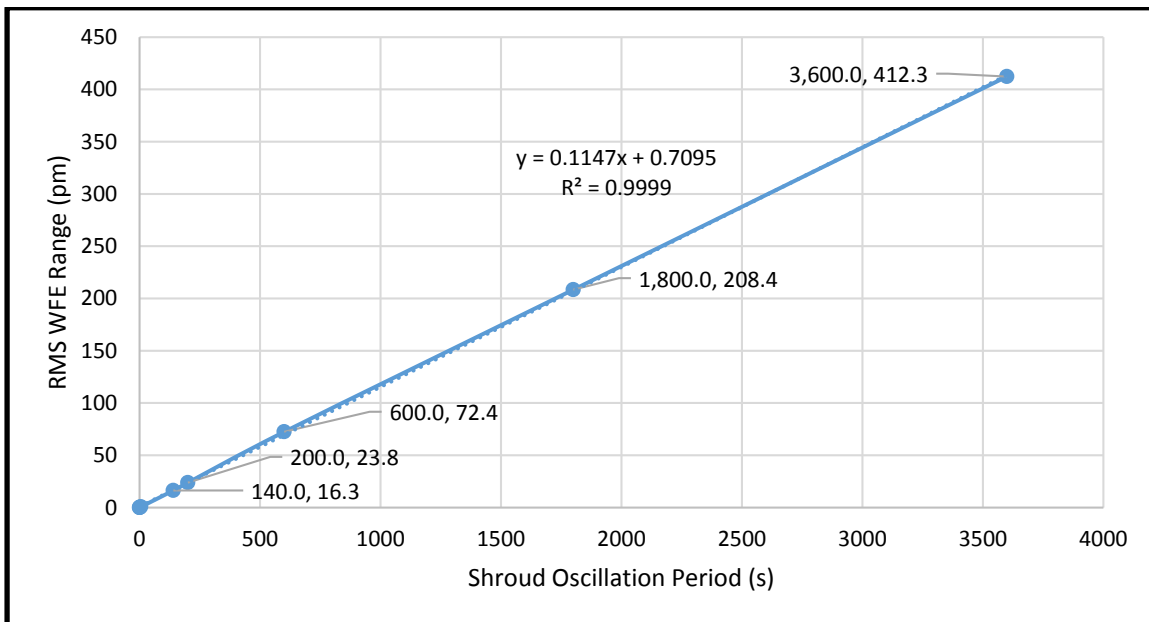
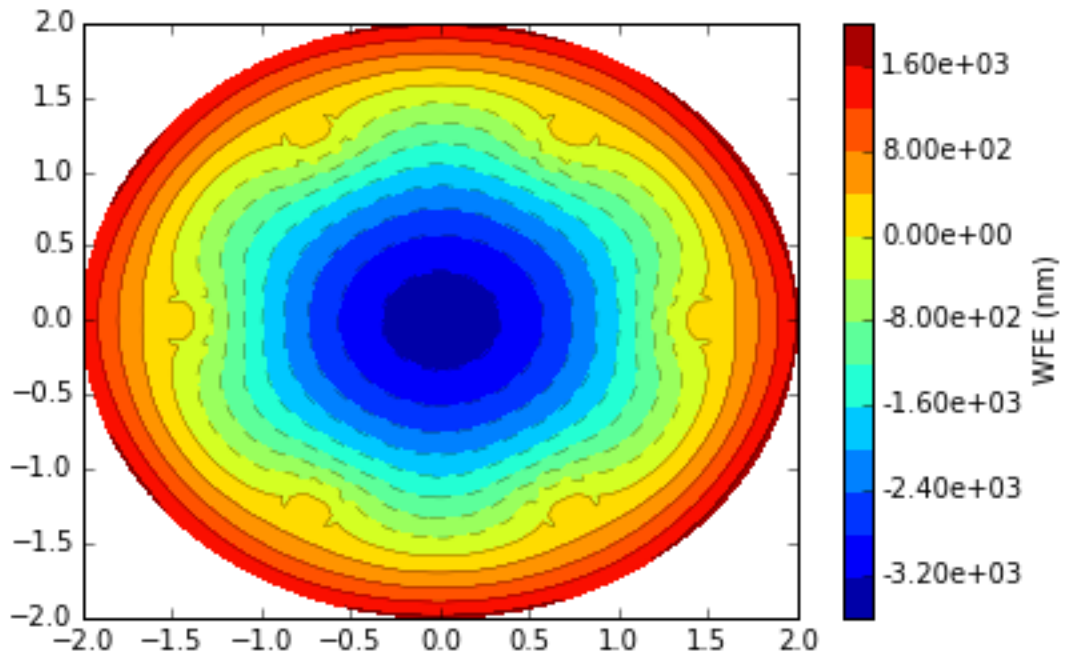**Figure 6: ACS Period versus RMS WFE Range**

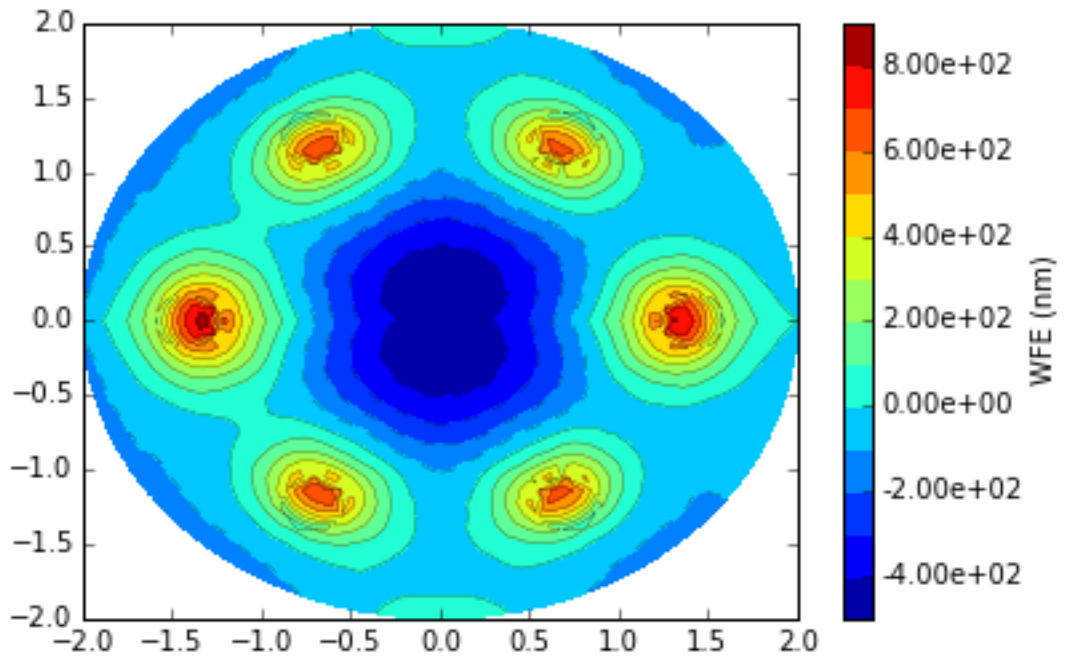**Figure 7: Sample WFE Contour Plot (50mK, 140s ACS)**

Figure 8: Sample WFE with first 6 Zernike Polynomials Removed (50mK, 140s ACS)

2.3.3. Model Conclusions

As the period of the ACS decreases, the RMS WFE Range decreases. This proves that an active control system with a quicker response will control the mirror better. This is an expected result that happens because faster oscillations in the boundary temperatures give the mirror less time to respond to the changes in boundary temperatures, causing the mirror to oscillate across a smaller range.

Figure 7 and Figure 8 show the WFE(x,y) on the primary mirror's surface and the WFE(x,y) after the first 6 Zernike Polynomials have been removed, respectively. The first 6 Zernike Polynomials are commonly removed by a closed loop wavefront control system. Some of the WFE shown here may be caused by the fact that the mirror is held by 6 fully constrained points in this analysis rather than a whiffletree or floating mirror mount. The fixture points are large contributors to WFE as shown in Figure 8. Analyses that include a kinematic mount are discussed in later sections, and the assumptions made here are consistent throughout these analyses and should not affect the nature of the relationships between the parameters and thermal WFE stability.

2.4.   Effect of Conductivity
2.4.1. Model Setup

The table below contains the values of key quantities in this model.

Table 4: Effect of Conductivity Analysis Settings

Material	ULE
Period of ACS	140s
Controllability of ACS	50mK
Density of Mirror Material	ULE Density
Emissivity	0.82
Thickness	Nominal
Conductivity	Varied

This model is made to determine the relationship between the conductivity of the mirror substrate's material and the primary mirror's RMS WFE Range. To achieve this, the model contains multiple cases which vary the conductivity of the material used in the mirror by multiplying the conductivity by 0.25, 0.5, 1, 2, 4, and 8. The base conductivity is the nominal ULE conductivity shown in Table 1.

2.4.2. Model Results

The results are summarized by comparing the normalized conductivity to the RMS WFE Range as shown in Figure 9.
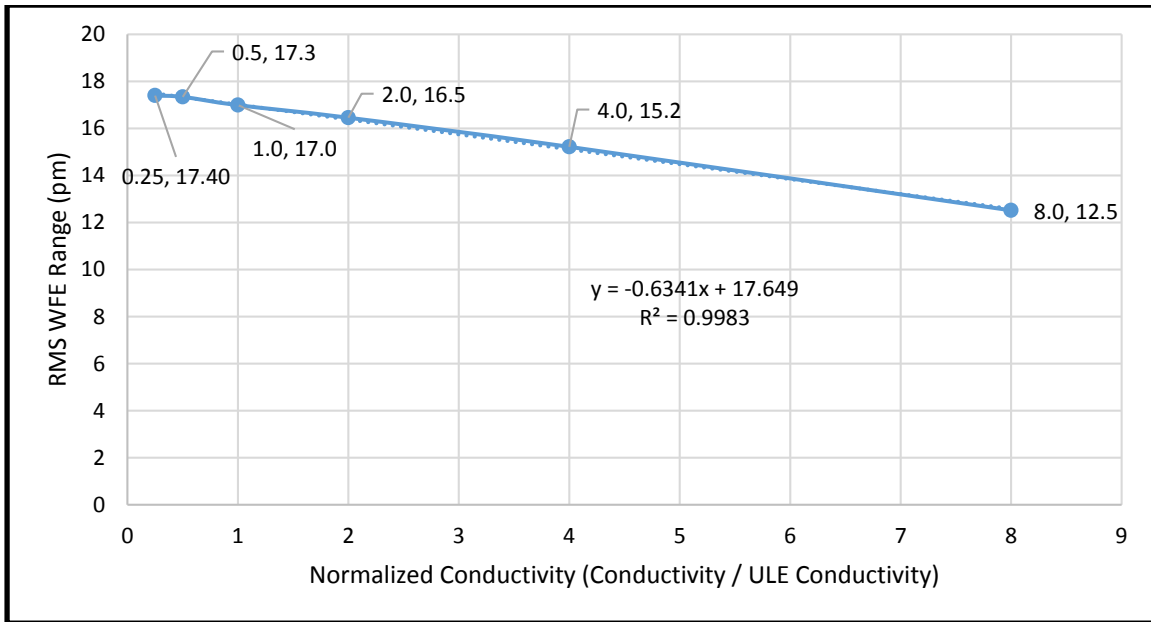
Figure 9: Normalized Conductivity versus RMS WFE Range

2.4.3. Model Conclusions

The results show that the relationship between conductivity and the RMS WFE Range is largely linear, though the line flattens as the conductivity becomes very small. The data points at 0.25 and 0.5 normalized conductivity were checked thoroughly due to this change in trends and no error in the calculation method was found, so it is thought that this change in the trend is real and potentially caused by conductivity becoming negligibly small as radiation takes over as the most dominate mode of heat transfer. The results above show that increasing the substrate's conductivity will cause a decrease in the RMS WFE Range. The RMS WFE Range will not be halved by a doubling of conductivity. This indicates that simultaneously doubling CTE and conductivity will result in an increase in the RMS WFE Range when a mirror is placed in an actively controlled shroud, so commonly used figures of merit that assume a cancellation of CTE with conductivity need to be rethought for stability analysis. These figures of merit include the steady state distortion coefficient (CTE/conductivity) and the transient distortion coefficient (CTE/thermal diffusivity). While these figures of merit are indicative of a substrate material's thermal qualities, this analysis shows that it is possible for a material with a low transient distortion coefficient to actually be worse than a material with a higher transient distortion coefficient.

2.5. Effect of Density and Controllability
2.5.1. Model Setup

The table below contains the values of key quantities in this model.

Table 5: Effect of Density and Controllability Analysis Settings

Material	ULE
Period of ACS	140s
Controllability of ACS	Varied
Density of Mirror Material	Varied
Emissivity	0.82
Thickness	Nominal
Conductivity	Nominal

9

The objective for this model is to determine how density and controllability couple to affect the RMS WFE Range of the mirror's optical surface. The Controllability is the amplitude of the sinusoidal temperature boundary condition on the telescope's shroud. The Controllability is set to 20, 30, 40, 50, and 60mK, and the density of the mirror is multiplied by 1, 2 and 3. Changing density demonstrates how heat capacity affects the stability of the mirror. Doubling specific heat is equivalent to doubling density because either action will double the heat capacity of the mirror.

2.5.2. Model Results

The results are summarized by plotting the shroud controllability versus the RMS WFE Range at each density as shown in Figure 10.
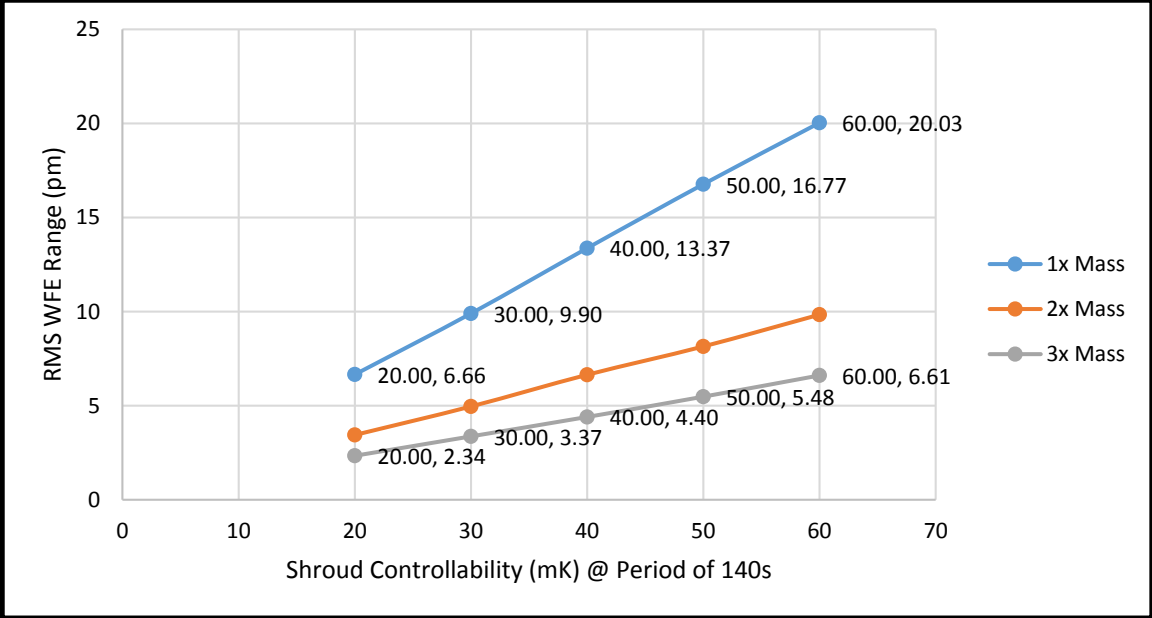

Figure 10: Shroud Controllability and Mass versus RMS WFE Range

2.5.3. Model Conclusions

A linear relationship is found between shroud controllability and RMS WFE Range and an inverse relationship is found between the material density and RMS WFE Range. The shroud controllability and density appear to affect the RMS WFE Range independently of one another with no coupling or interaction effects. The variability of the results are found to be very small, and the trends show no sign of changing from their expected relationships. The results show that it is best that the shroud's temperature is tightly controlled (as expected) and that more mass slows the rate at which the mirror change's temperature. The inverse relationship between density and RMS WFE Range agrees well with the results in the Sheet Thickness analysis because both indicate that mirror mass has an inverse relationship with the shroud's RMS WFE Range. An object's time constant is directly proportional to its mass and this indicates that the mirror's time constant may be inversely proportional to the RMS WFE Range of that mirror inside of a given ACS.

2.6. Effect of Sheet Thickness
2.6.1. Model Setup

The table below contains the values of key quantities in this model.

Table 6: Effect of Sheet Thickness Analysis Settings

Material	ULE
Period of ACS	140s
Controllability of ACS	50mK
Density of Mirror Material	ULE Density
Emissivity	0.82
Sheet Thickness	Varied
Conductivity	Nominal

This model varies the thickness of all elements in the mirror model to determine how the change in thickness of the mirror front face, back face, and ribs affect the mirror's thermal stability. This model gives results that represent changes similar to an increase in density and conductivity, but that are more realistically achievable by design. The thicknesses throughout the mirror model were multiplied by 0.5, 1, 2, and 4 to determine how thicknesses affect the performance of the mirror.

2.6.2. Model Results

The results are summarized by comparing the Normalized Sheet Thickness to the RMS WFE Range. The Normalized Sheet Thickness is the value by which all sheet thicknesses (front face, back face, and rib thicknesses) are multiplied to obtain the results shown in Figure 11.

$$y = 18.063/x - 0.31553x$$
$$R^2 = 0.9991$$
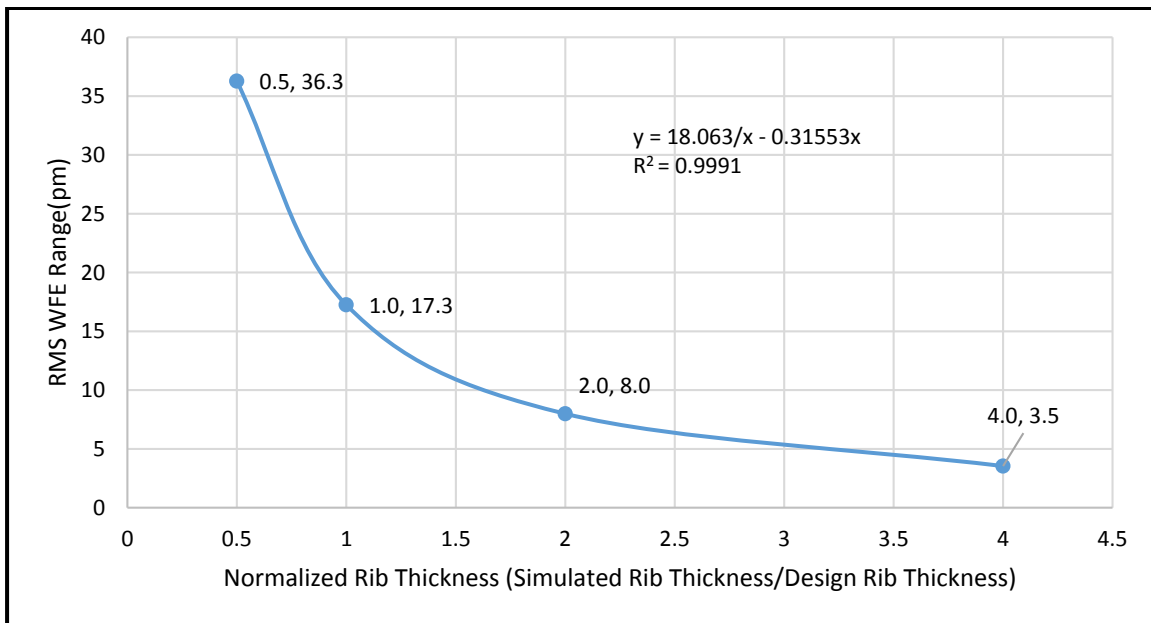
Figure 11: Normalized Sheet Thickness versus RMS WFE Range

2.6.3. Model Conclusions

An increase in sheet thickness results in an increase in the mirror's thermal stability. The relationship between sheet thickness and RMS WFE Range is found to be nonlinear. Increasing the thickness of the ribs, sides, front, and back faces

11

linearly increases mass, but nonlinearly increases stability. This means that trade of greater mass for greater stability will be very advantageous and appealing when the sheets are thin but will become less appealing as the sheets become thicker.

An increase in sheet thickness results in both an increase in mass and an increase in the in-plane conductance. There is an inverse relationship between the increase in mass in the primary mirror and the RMS WFE range of the primary mirror as shown in section 2.5. There is a negative, linear relationship between the increase in conductance and the RMS WFE range as shown in section 2.4. The chart above shows a nearly inverse relationship between normalized sheet thickness and RMS WFE range because the overall effect of increasing sheet thickness is the summation of the effect of increasing mass with a fraction of the effect of increasing conductance. Only a fraction of the effect of increasing conductance is seen in the chart above because the conductance is increased in the plane of the sheets while the conductance across the sheets is actually decreased by the increased thickness. Increasing sheet thickness has very nearly half the conductance related effect on the RMS WFE range as increasing conductivity. This is shown by the fact that the best fit curve shown in Figure 11 has a linear coefficient of -0.316, while the linear coefficient in Figure 9 is -0.634. Based on the graph above, it is clear that the increase in mass has a much greater effect on the RMS WFE range than the increase in conductance for a material that has a conductivity to density ratio similar to ULE's.

2.7. Effect of Emissivity
2.7.1. Model Setup

The table below contains the values of key quantities in this model.

Table 7: Effect of Emissivity Analysis Settings

Material	ULE
Period of ACS	140s
Controllability of ACS	20mK
Density of Mirror Material	ULE Density
Emissivity	Varied
Thickness	Nominal
Conductivity	Nominal

The emissivity of the optical face of the mirror remained constant at 0.03 to represent a highly reflective surface in the IR. The sides of the mirror are covered in MLI and the optical properties there remained constant as well. The mirror surfaces that faced the heater and the mirror's inward facing surfaces are the surfaces whose emissivity is varied. It should be noted that the controllability of the ACS is 20mK in this analysis, while it was 50mK everywhere else, making it hard to compare this trade studies to the others, but possible by using the knowledge gained in the controllability trade study above which showed that we simply need to multiply the RMS WFE range's in this chart by 50mk/20mk (2.5) to compare this chart the previous charts.

2.7.2. Model Results

The results are summarized by plotting the emissivity versus the RMS WFE Range as shown in Figure 12.
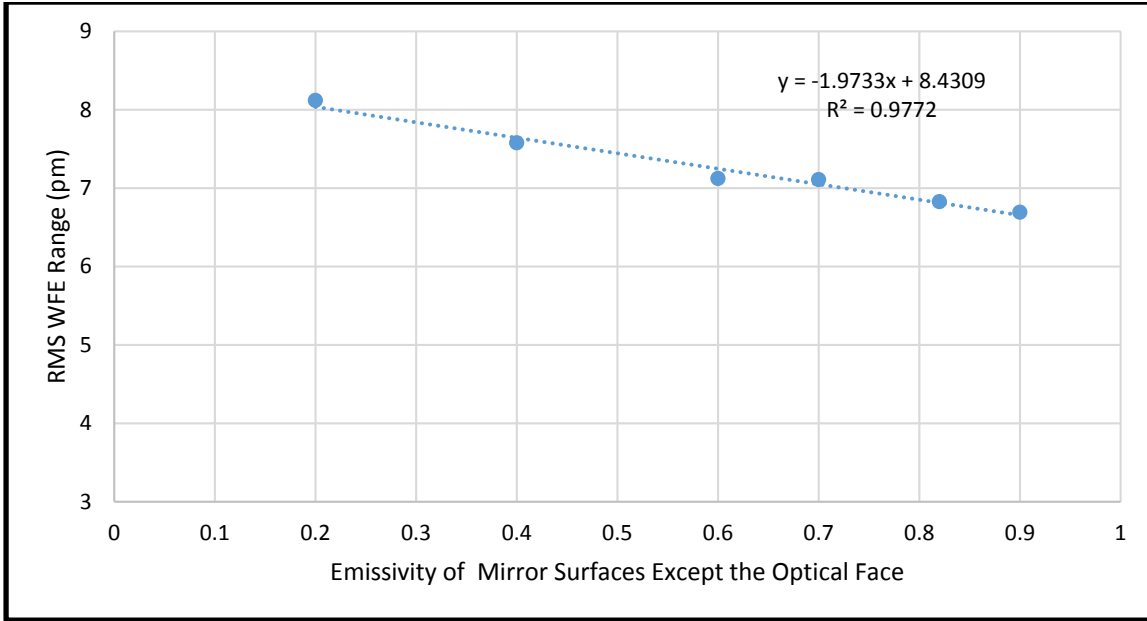
Figure 12: Mirror Material Emissivity versus RMS WFE Range

2.7.3. Model Conclusions

The results show that as the mirror surface's emissivity increases, the mirror becomes easier to control thermally. There is variation from the trend line in this analysis, and this is attributed to error in ray tracing calculations. In all of the previous analyses, the radiative connections are determined by random ray tracing only once, and therefore, the radiation connections are constant for each case. In this analysis, the ray tracing is rerun for every case, because the emissivity is varying and the emissivity value affects the results of ray tracing. For reference, 50,000 rays per node were used in this analysis. Despite the variability from ray tracing, a line fits the data points very well with a high R^2 value which indicates that the ray tracing calculations are well converged in these analyses at 50,000 rays per node.

The results shown here are similar to the results seen in the conductivity versus RMS WFE range analysis. These general trend indicates that conductance between the periphery of the mirror and its interior can be increased to decrease the RMS WFE range of a mirror.

2.8. Effect of Material
2.8.1. Model Setup

The table below contains the values of key quantities in this model.

Table 8: Effect of Material Analysis Settings

| Material	Varied
Period of ACS	140s
Controllability of ACS	50mK
Density of Mirror Material	Material Density
Emissivity	Material Emissivity
Thickness	Nominal
Conductivity	Material Conductivity

13

The mirror material is varied between Silicon Carbide, ULE, and Zerodur to see how material type alone affects the stability of the mirror. The material properties for these three materials are shown below. These properties are valid at room temperature which is near the temperature that the mirror will be during this analysis. The CTE properties used for ULE and Zerodur are actually spatially inhomogeneous. The maximum CTE value is used throughout the mirrors for simplicity.

Table 9: Mirror Material Properties

Material	Conductivity (W/m/K)	Specific Heat (J/kg/K)	Density (kg/m³)	Emissivity	CTE (1/K)
ULE	1.31	766	2210	0.82	30×10^{-9}
Silicon Carbide	180	750	3100	0.9	2.2×10^{-6}
Zerodur	1.46	800	2530	0.9	7×10^{-9}

2.8.2. Model Results

The model results are summarized by comparing the material to the RMS WFE range as shown in Figure 13.
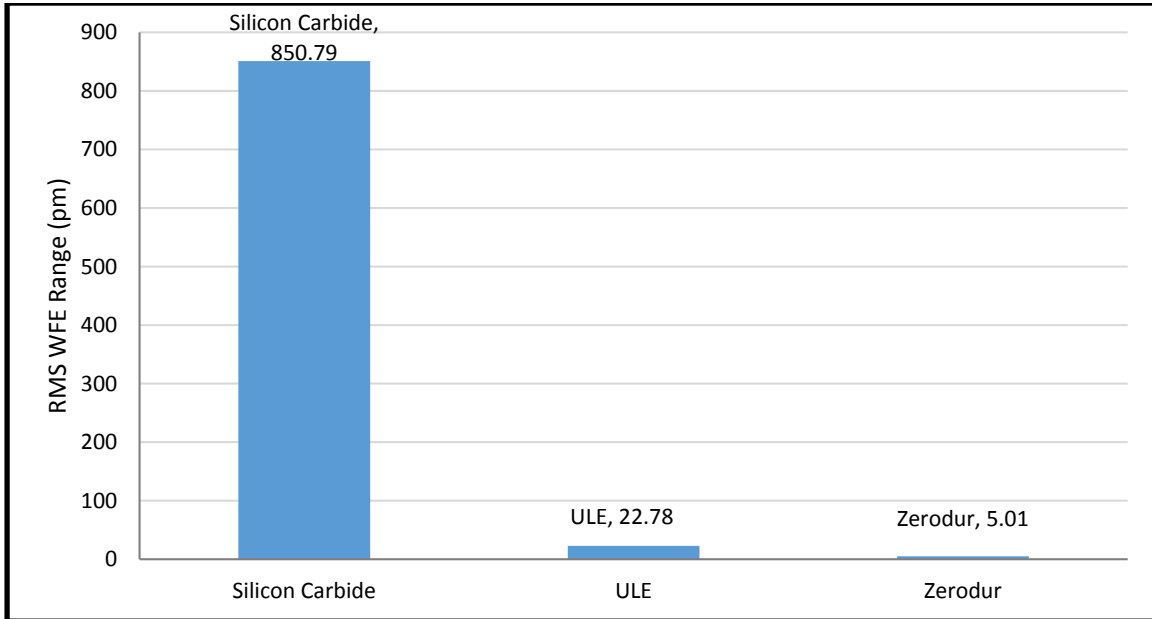
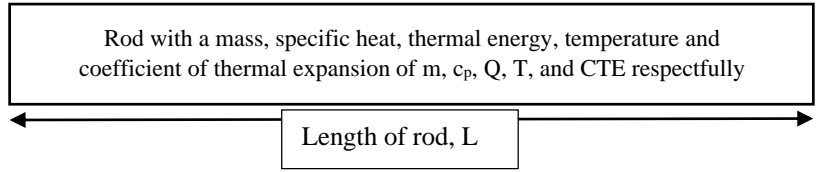**Figure 13: Material versus RMS WFE Range**

2.8.3. Model Conclusions

The mirror made from Silicon Carbide is the least thermally stable because its CTE is much larger than either of the other materials'. However, it should be noted that these material comparisons only varied material and did not change the mirror design to accommodate the new material so the mirror designs are not equivalent in other ways such as stiffness, weight, and cost. A Silicon Carbide mirror could have thinner sheets because of its greater stiffness, which would add more thermally induced RMS WFE as shown in Figure 11. Because of this, Silicon Carbide would require an even more advanced thermal control system if it is light weighted based solely on dynamic and structural concerns. In this simplified analysis, Zerodur out-performs ULE due to its higher conductivity, greater heat capacity, higher emissivity, and lower CTE.

2.9. Closed-Form Analysis

2.9.1. Setup and Analysis

A one-dimensional rod is modelled as a single control volume to find a relationship between the rate of thermal deformation and the material properties of the rod. This analysis is done because

Rod with a mass, specific heat, thermal energy, temperature and coefficient of thermal expansion of m, c_P, Q, T, and CTE respectfully

Length of rod, L

Figure 14: Closed-Form Analysis Geometry

finding a thermally induced strain rate in the rod gives insight into which properties of an object affect its thermally induced strain rate. A description of the energy stored in the rod is shown in equation 1.[2]

$$Q = mc_pT \qquad \text{Equation 1}$$

By taking the derivative of both sides with respect to time and assuming a constant specific heat and mass, we get equation 2 shown below.

$$\frac{dQ}{dt} = mc_p\frac{dT}{dt} \qquad \text{Equation 2}$$

Linear expansion is described by equation 3 below.[3] The derivative of equation 3 with respect to time yields equation 4. CTE and length's time dependence are sufficiently small to be considered second order effects and their derivate terms are removed following the application of the product rule. Equation 4 is placed into equation 2 and rearranged to yield equation 5.

$$(\textbf{CTE})\textbf{\textit{L}}\boldsymbol{\Delta}\textbf{\textit{T}} = \boldsymbol{\Delta}\textbf{\textit{L}} \qquad \text{Equation 3}$$

$$(\textbf{CTE})\textbf{\textit{L}}\frac{dT}{dt} = \frac{dL}{dt} \qquad \text{Equation 4}$$

$$\frac{dL}{dt} = \frac{(\textbf{CTE})L}{V\rho c_p}\frac{dQ}{dt} \qquad \text{Equation 5}$$

2.9.2. Conclusions

Equation 5 shows the rod's thermal expansion rate will be linearly proportional to its length, coefficient of thermal expansion, and heating rate. The rod's growth rate will be inversely proportional to its heat capacity. The parameters that affect the thermal expansion rate can be divided into material dependent and geometry dependent terms. The material dependent terms are the CTE, specific heat, and density. The geometry dependent terms are the volume, length, and heating rate.

From this simplified analysis, it can be inferred that a primary mirror's thermally induced surface figure error will grow in a similar fashion. The rate of deformation in the optical axis will increase with increasing mirror depth, coefficient of thermal expansion, and heating rate and decrease with increasing heat capacity. Dynamic changes in heating rate can be reduced by surrounding the mirror with insulation and lowering the emissivity of the shroud around the mirror.

3. Summarized Conclusions

A balance must be struck between requirements levied on the active control system, requirements levied on the primary mirror, and requirements levied elsewhere. Increasing the accuracy or frequency of the active control system has a linear effect on the primary mirror's RMS WFE range. If the ACS is perfectly accurate or controlled at an infinite frequency, the mirror will not deform due to a change in its own temperature. The mirror may be designed to be stable as well. If the mirror has an infinite mass or zero CTE, the primary mirror will not deform due to its own temperature changes. This is confirmed by numerical models as well as a closed form analysis. A mirror substrate with higher conductivity and emissivity will have greater stability, but the mirror's geometry impacts how much emissivity and conductivity affect the mirror's stability. The numerical models and the closed form solution both agree that stability will be inversely related to

heat capacity. The analytical model shows deformation rates will be linearly related to the CTE of the mirror substrate. From this work, a new material characterization number is suggested which describes the rate of deformation of a material under a given heat input. The value of this number is given below:

$$\text{Massive Active Optothermal Stability } MAOS = \frac{c_p \rho}{CTE}$$

A material with a high MAOS will strain slowly due to a change in the thermal environment and a material with a low MAOS will strain quickly in response to a change in the thermal environment. For the application analyzed in this paper, i.e. an optic enclosed in an actively controlled thermal environment, a large MAOS is preferred. However, mass is bad from structural, dynamic, launch, and other standpoints. For this reason, the AOS is introduced and defined below:

$$\text{Active Optothermal Stability } AOS = \frac{c_p}{CTE}$$

The table below relates commonly used substrate materials and their thermal stability number.

Table 10: Thermal stability quality of commonly used substrate materials

Material	Massive Active Optothermal Stability (TJ/m^3)	Active Optothermal Stability (GJ/kg)	Specific heat (J/kg/K)	Density (kg/m^3)	Coefficient of thermal expansion (1/K)
Fused silica	2.91	1.32	741	2202	5.60E-07
ULE 7971	112	51.1	766	2200	1.50E-08
Zerodur	83.1	32.8	821	2530	2.50E-08
Cer-Vit C-101	140	56.0	840	2500	1.50E-08
Beryllium I-70A	0.298	0.161	1820	1850	1.13E-05
Aluminum 6061-T6	0.113	0.042	960	2710	2.30E-05
Silicon Carbide CVD	0.936	0.292	700	3210	2.40E-06
Borosilicate crown E6	0.595	0.255	830	2330	3.25E-06

4. Optimized Shroud and Heater Temperature Profiles
4.1. Model Layout

4.1.1. Shroud and Scarf

Like in the previous analyses, a Kepler-like space telescope is modeled as shown in Figure 15. The outward facing surfaces of the shroud and scarf are covered in MLI (effective emissivity of 0.002; emissivity 0.82; absorptivity 0.45) and the inward facing surfaces are covered with black paint (emissivity of 0.91) to prevent stray light from affecting the telescope's optical performance. The height of the shroud is 8.15 m and its diameter is 4.3 m. The shroud's temperature is set to a boundary condition that varies as a function of axial location. In this analysis, the temperature distribution is constrained to a simple quadratic equation shown below where a, b, and c are fitting parameters and z is the axial distance from the shroud's base:

$$T(z) = a + bz + cz^2$$

The scarf's temperature is treated as though there is no active control on it and it is allowed to change based on its thermal connection to the rest of the telescope and the space environment. No solar load is applied to the scarf.

4.1.2. Heated Plate

A heated plate is behind the primary mirror as shown the case in the previous analyses and shown in Figure 2. The heated plate is made out of Aluminum 6061-T6. The surface of the heated plate that faces the telescope's shroud is covered in MLI and the mirror facing surface is covered in an optical coating that has an emissivity of 0.9. The heated plate's temperature varies radially and follows a quadratic equation shown below where r is the radial distance from the center of the heater and d, e, and f are fitting parameters:

$$T(r) = d + ez + fz^2$$

4.1.3. Mirror

The base mirror from the previous trade studies is also used in this analysis. The mirror remains 4m, circular, closed back, ULE and with the same light-weighting pattern throughout the analysis as shown in Figure 16. The same ULE properties are used as those described in Table 1.

4.1.4. Environment

The telescope is placed in space and the space boundary temperature is set to the cosmic microwave background temperature of 2.7K. No Solar loading is applied to the scarf or shroud. The shroud is set to a boundary temperature so thermal loads cannot affect its temperature.

4.1.5. Optimization Analysis

An optimization algorithm varies the fitting parameters a, b, c, d, e, and f and runs steady state analyses to find the fitting parameters that
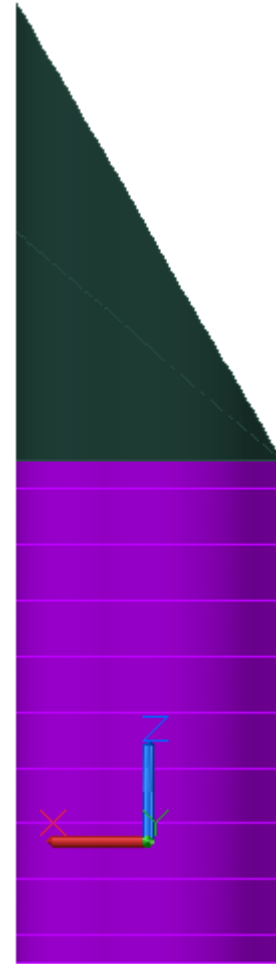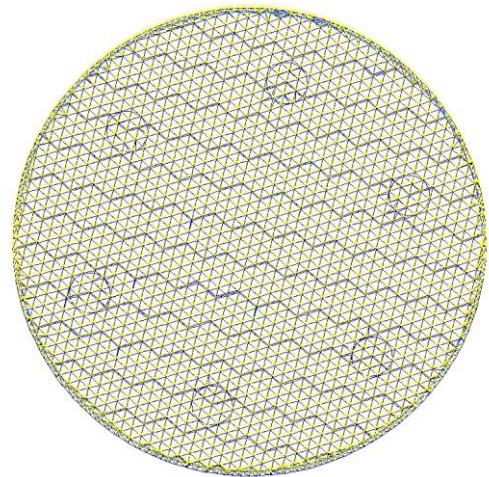

Figure 15: Shroud & Scarf

Figure 16: Mirror in Wireframe View

minimize the uncorrected RMS WFE at steady state. A close approximation of WFE can be found by doubling the deflections in the z direction on the mirror's front surface.[1] This method is used to find the WFE distribution and the RMS of these values is determined to get the uncorrected RMS WFE. It should be noted that these terms are considered uncorrected because they do not remove any Zernike shapes.

4.2. Results

The minimum uncorrected RMS WFE was found to be 6.6 nm with the distribution shown in Figure 17. Note that a uniform CTE of $30 \times 10^{-9}/°C$. A ULE mirror would in reality have an average CTE much lower than the used CTE. This is a worst case analysis. The temperature span on the primary mirror is around 1°C as shown in Figure 18. The temperature distribution in the shroud and heater are shown in Figure 19 and Figure 20 respectively.
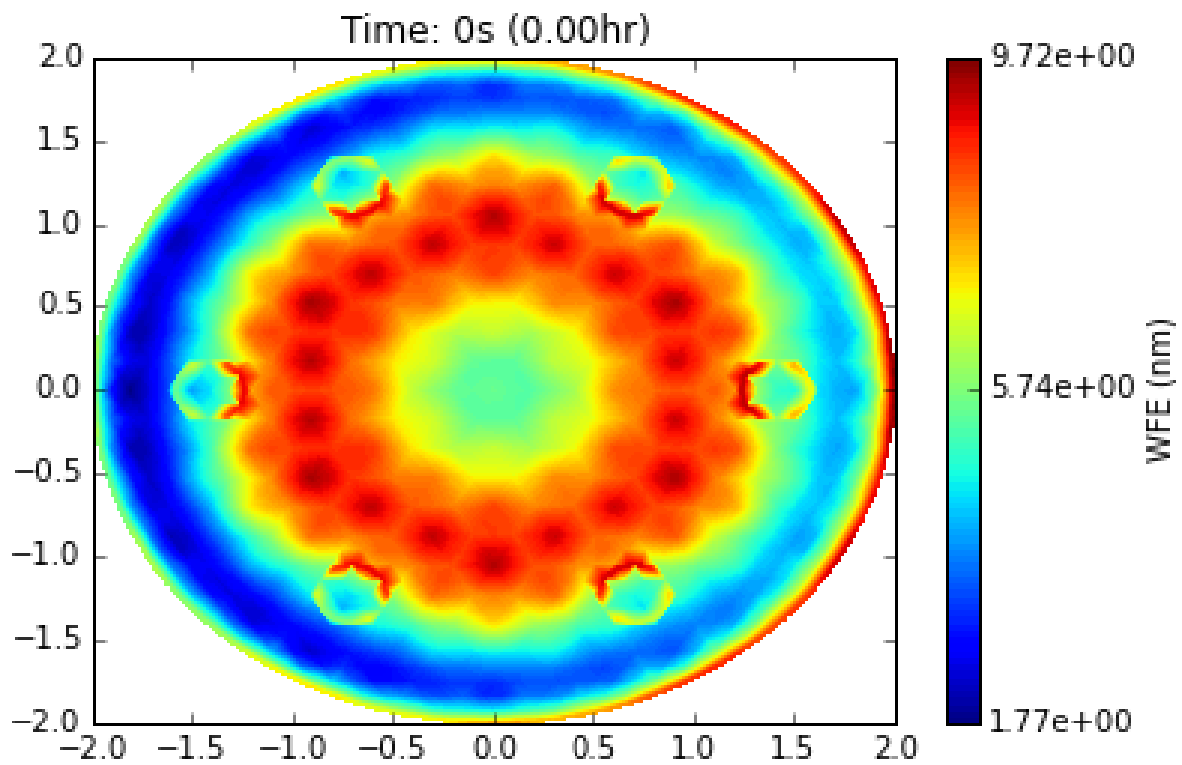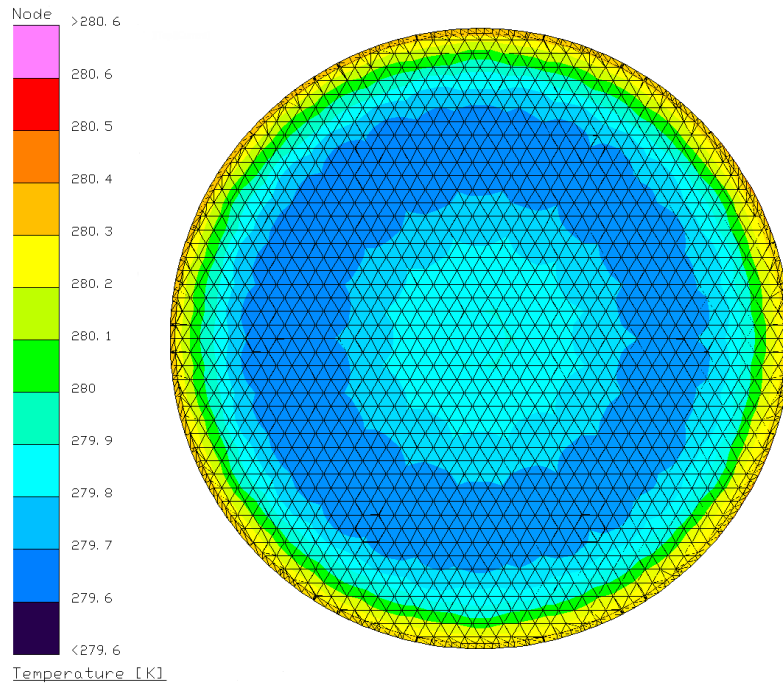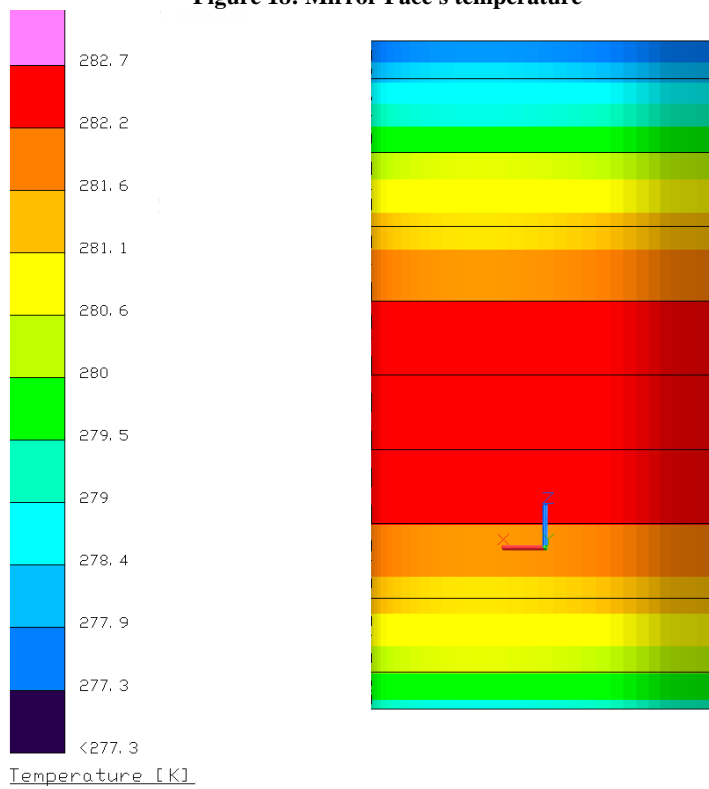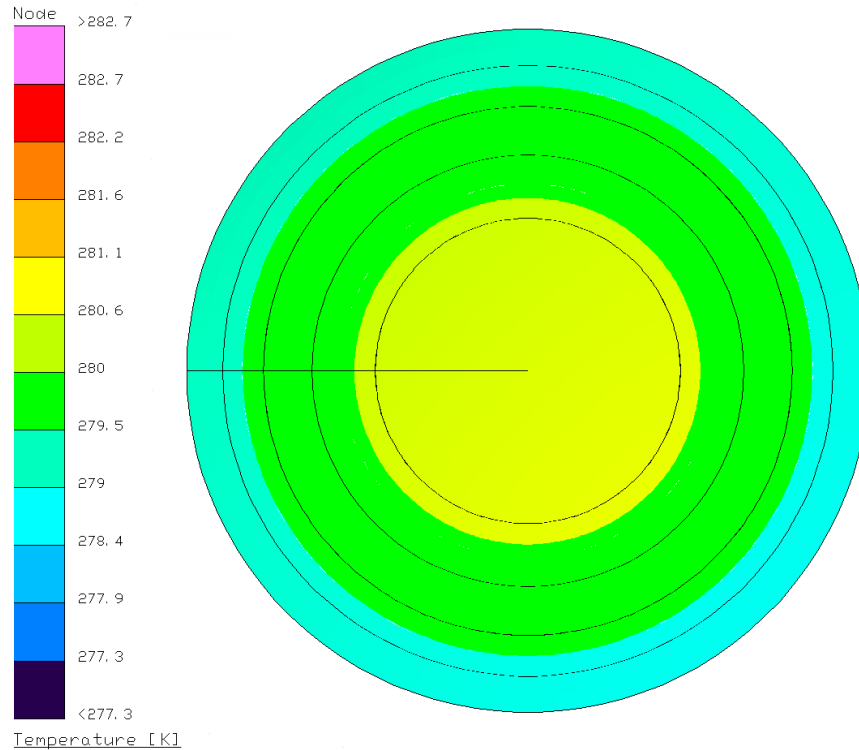

Figure 17: RMS WFE of Optimized Control System

18

Figure 18: Mirror Face's temperature

Figure 19: Shroud Temperature Distribution

Figure 20: Heated Plate Temperature Distribution

4.3. Conclusions

The WFE appears to have large contributions from spherical, piston, and tilt aberrations. The analysis' pad effects are also apparent in the WFE plot. Asymmetry in the mirror's temperature is caused by the scarf's asymmetry. The best-found solution shows a heater that is hot in the center and cooler on the outsides. The higher temperature in the center of the heater provides greater heat to the mirror's center which offsets the mirror's greater view to space at its center. The shroud has a temperature close to the mirror's set temperature at the mirror's axial location and higher temperatures in the middle of the shroud. The temperature distribution in the shroud is based upon the balance between the mirror face's view factor to space and to the sides of the shroud.

References

[1] Yoder, P.R., *Opto-Mechanical Systems Design*, 2nd ed., Marcel Dekker, New York, NY (1993).

[2] Incropera, F.P., *Fundamentals of Heat and Mass Transfer*, 6th ed., John Wiley & Sons, Hoboken, NJ, 257, (2007).

[3] Tester, J.W., *Thermodynamics and Its Applications*, 3rd ed., Prentice Hall PTR, Upper Saddle River, NJ, 240-241, (1997).